

N74-19451

15. Motion of a Fragment in Disturbed Air Behind a Meteor Body

V. PADEVĚT

*Astronomical Institute of Czechoslovak Academy of Sciences
Ondřejov, Czechoslovakia*

EVEN IF WE USE the classical physical theory of meteors, there may still be some possibility for agreement between observations and theory. The effect of disturbed air behind the main body on the motion and ablation of fragments has not yet been considered. This effect may have important consequences, observed partly as the difference between the photometrically and the dynamically determined masses of the meteor body. By use of extreme mathematical conditions, this difference can be made to reach orders of magnitude during the latter part of the trajectory. However, the physical interpretation is considered only roughly in this paper, and the computed model needs further improvement. But the main purpose here—finding an important effect for the explanation of the discrepancy between the dynamic and the photometric masses, especially for large bodies—has been achieved.

ASSUMPTIONS

The mathematical model used here contains the following simplifications: If a single meteor body with velocity v and radius R deposits its mass only in small fragments of radius R_f , the ablation of a spherical stony parent body is given by the following equations:

$$\frac{dR}{dt} = \frac{-\Lambda(t)\rho v^3}{8Q\rho_m} \quad (1)$$

$$\frac{dv}{dt} = \frac{-3\Gamma\rho v^2}{4R\rho_m} \quad (2)$$

$$\frac{d\rho}{dt} = b\rho v \cos z_R \quad (3)$$

and

$$\Lambda(t) = A_0 + A_1 \cdot t + A_2 \cdot t^2 \quad (4)$$

where $Q = c \cdot \tau_c$, Λ is the heat-transfer coefficient, ρ is the density of the free atmosphere, ρ_m is the density of the meteoroids, c is the specific heat of the meteoroid, b is the reciprocal of the density scale height of the atmosphere, and the temperature of the meteoroid outside the atmosphere is taken as zero. Equation (4) is simply an approximate polynomial expansion of second degree in time for the heat-transfer coefficient.

The following idealized history of each small fragment is assumed. The fragment leaves the parent body with temperature τ_c . Starting with this temperature, the fragment is heated to the evaporation temperature, cooling by radiation being taken into account. Isothermal heating is assumed for such small fragments, and the following equations are thus valid for the first part of the trajectory:

$$\frac{c \cdot \rho_m R_f}{3} \frac{dT}{dt} + \sigma_R (T^4 - T_0^4) = \frac{\Lambda_f \rho_f v^3}{8} \quad (5)$$

$$\frac{dv}{dt} = \frac{-3\Gamma\rho_f v^2}{4R_f\rho_m} \quad (6)$$

$$\frac{dH}{dt} = -v \cos z_R \quad (7)$$

$$\rho_f = \rho - F(H_0 - H) \quad (8)$$

Here, σ_R is the Stefan-Boltzmann constant, Λ_f the heat-transfer coefficient for fragments, and Γ the drag coefficient.

We deal with a very simplified case in this paper, the air density at height H being the only disturbed entity; the density in the wake is denoted by ρ_f . In equation (8), F describes this disturbance. The function F also depends on the height of fragment separation, H_0 ; it has two extreme values: $F=0$ if the atmosphere behind the parent body is not disturbed, and $F=\rho$ if there is a vacuum behind.

After being heated to the evaporation temperature, the fragment starts the second part of its trajectory. The temperature is determined by radiation, vaporization, and aerodynamic heating. Mass loss and luminosity occur until the energy flux is balanced by radiation. The second part of the fragment's trajectory can be described by the following equation:

$$\frac{dR_f}{dt} = - \frac{\Lambda_f \rho_f v^3 - 4\sigma_R (T^4 - T_0^4)}{8Q_f \rho_m} \quad (9)$$

and by equations (6), (7), and (8). Here, Q_f is the heat of ablation of vapors from the fragment. Visual radiated luminosity I_f belonging to one fragment is then described in terms of the luminous efficiency coefficient τ_0 by

$$\begin{aligned} I_f = & \frac{1}{2} A \left(\frac{4}{3} \pi \rho_m \right)^{2/3} \tau_0 v^3 R_f^2 (H_0) \\ & \times \left[\sigma_f \Gamma \rho_f v^3 - \frac{4\sigma_R (T^4 - T_0^4)}{Q_f} \right] \\ & \times \exp \left[- \frac{\sigma_f}{3} (v_{H_0}^2 - v^2) \right] \quad (10) \end{aligned}$$

where

$$\sigma_f \equiv \frac{\Lambda_f}{2\Gamma Q_f}$$

Also, A denotes the shape factor.

PROCEDURE USED

The total light intensity at a given height H_m is the sum of all the partial intensities from all the fragments that separated from the parent body at heights $H \geq H_m$. It is clear that the fragments that separated within heights $H_1 > H \geq H_m$

are not shining, because they are not yet heated enough. The beginning of the light curve is taken at the height corresponding to the air density ρ_B computed for the ending of the preheating period according to the formula by Ceplecha and Padevët (1961):

$$\rho_B = \frac{8\lambda\tau(R)}{av_\infty^3 R} \left(WR \frac{e^{WR} + e^{-WR}}{e^{WR} - e^{-WR}} - 1 \right) \quad (11)$$

where $W = (b \cos z_R \cdot v_\infty)^{1/2} / \beta$, β^2 is the thermal diffusivity, λ is the thermal conductivity of the meteoroid, τ is the temperature at which structural failure occurs, and a is the accommodation coefficient. The end of the light curve is defined to be at the height where the velocity has decreased to 5 km/s.

The dynamic and photometric masses can now be computed and compared by means of the same procedures as for observed meteors. Equations (1) to (4) are used to find the radius and thus the mass of the body, and the conventional luminous equation

$$m_p(t) = \frac{2}{\tau_0} \int_t^{t_{\text{end}}} \frac{I(t')}{v^3} dt' + m_{\text{end}} \quad (12)$$

is used to determine the photometric mass. Here, v is the velocity of the parent body and I is the instantaneous intensity. The integration constant m_{end} was taken as the dynamically determined mass at the terminal point.

The change of air density behind the parent body might alter the computed photometric masses, but there is no need to attain higher values than those in the paper by McCrosky and Ceplecha (1970). However, if, for example, a constant factor for decreasing the density behind the main body is used, this undesired effect happens. But such a simple model for the function F does not correspond even to a primitive physical guess. We would expect a decrease of the disturbance farther behind the meteor body, terminating with the density of the undisturbed atmosphere. It seems that each realistic model of the disturbance will result in a decrease of luminosity originating from one fragment. In an attempt to increase the photometric mass, we should find a model of the disturbance that would decrease the level of the photometric mass as little as possible and we should look for another

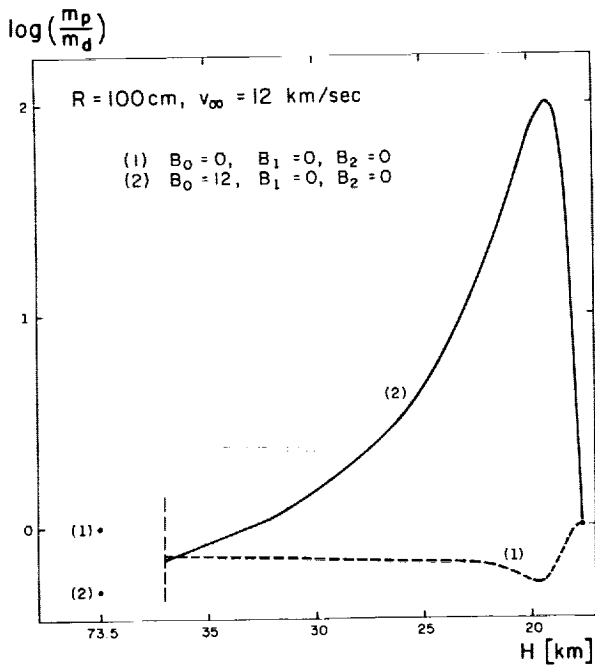


FIGURE 1.—Logarithm of the ratio of the photometric mass m_p to the dynamical mass m_d for an initial radius $R_\infty = 100$ cm and an initial velocity $v_\infty = 12$ km/s.

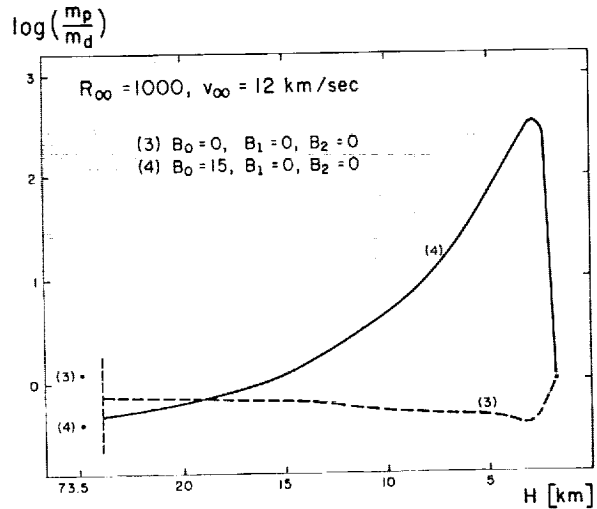


FIGURE 2.—Logarithm of the ratio of the photometric mass m_p to the dynamical mass m_d for an initial radius $R_\infty = 1000$ cm and an initial velocity $v_\infty = 12$ km/s.

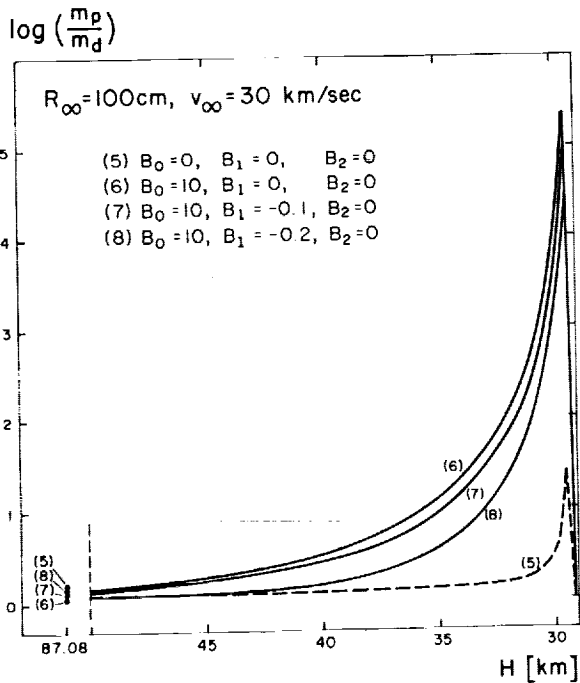


FIGURE 3.—Logarithm of the ratio of the photometric mass m_p to the dynamical mass m_d for an initial radius $R_\infty = 100$ cm and an initial velocity $v_\infty = 30$ km/s.

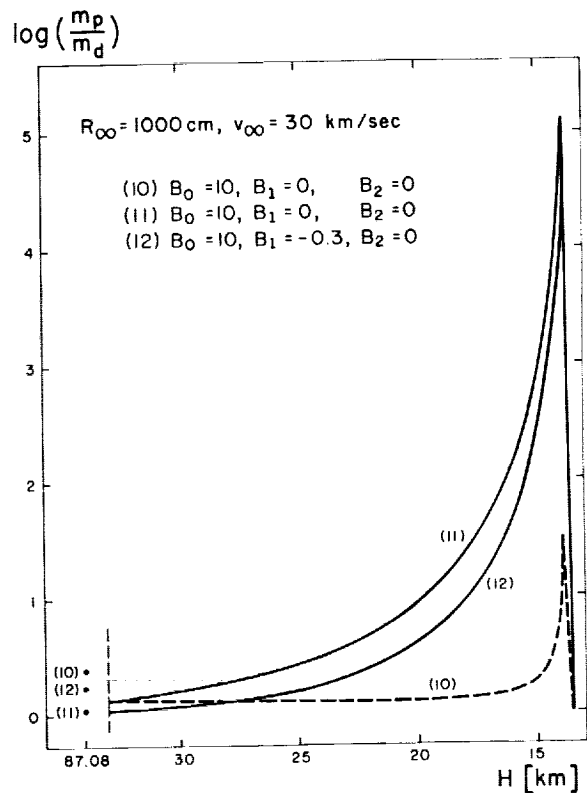


FIGURE 4.—Logarithm of the ratio of the photometric mass m_p to the dynamical mass m_d for an initial radius $R_\infty = 1000$ cm and an initial velocity $v_\infty = 30$ km/s.

effect strong enough to increase the level. The first condition may be met by a rather extreme and simple function—the discontinuous function $F = \rho$ for an interval of $H_0 > H > H_2$, and $F = 0$ for an interval of $H_2 \geq H \geq H_m$. The fragments begin by moving in vacuum but cannot move ahead of the decelerating parent body. As an extreme case, we can imagine that the fragments are moving in a trap close behind the body, departing at height H_2 . This extreme choice of the function F serves the computations well as the first approximation of some more realistic model. The real function should start from a value very close to the air density (almost vacuum), followed by a steep change that is represented here by the discontinuous jump to zero. All our preliminary computations used this discontinuous function.

An additional parameter now is the number of fragments crossing the discontinuity in the air density at a given height H_m . If the discontinuous function F is as above, only one change results: The height of the separation of the corresponding fragment will be higher than in the case without any disturbance. But we are interested in differences of orders of magnitude, and this is not possible with the above model with Λ constant. On the other hand, if we assume that Λ decreases with time, a steep decrease of the main-body mass results during the second part of the trajectory. Generally speaking, the decrease of Λ with time can be expected from the physical point of view.

RESULTS

Until now, only a limited number of cases have been computed. The numerical choice of parameters was made rather arbitrarily, with only great differences between the computed photometric and the computed dynamic masses being ac-

cepted. We can guess that the differences will be less after more physical factors are included, but the computed examples illustrate the general situation well.

Using the above model, we can explain the great difference between the dynamic and the photometric mass during the second part of the trajectory, if we assume chondritic densities for the body. As a function of time, the difference between the two masses is less in the first part of the trajectory and becomes greater at the end (see figs. 1 to 4).

COMMENTS

$D = B_0 + B_1 \cdot H_2 + B_2 \cdot H_2^2$ is the difference in height in kilometers between the fragment separation (H_0) and that of departure from the trap (H_2).

Numerical parameters used for computation of the values in tables 1 to 4 (cgs) are as follows:

a	= 1
A	= 1.21
b	= $1.6 \times 10^{-6} \text{ cm}^{-1}$
c	= $10^7 \text{ cm}^2 \text{ s}^{-2} \text{ deg}^{-1}$
Q_f	= $8 \times 10^{10} \text{ cm}^2 \text{ s}^{-2}$
initial R_f	= 0.01 cm
T_0	= 0° K
T_B	= 2580° K
$\cos z_R$	= 1
Γ	= 0.5
λ	= $3 \times 10^5 \text{ g cm s}^{-3} \text{ deg}^{-1}$
ρ_m	= 3.5 g cm^{-3}
σ_f	= $\frac{\Lambda_f}{2\Gamma Q_f} = 2 \times 10^{-12} \text{ cm}^{-2} \text{ s}^{-2}$
τ_c	= 600° C

The results do not depend on the value τ_0 .

REFERENCES

- CEPLECHA, Z., AND PADEVĚT, V., 1961. The beginning of rapid evaporation of meteors of different dimensions, *Bull. Astron. Inst. Czech.*, **12**, 191–195.
- MCCROSKY, R. E., AND CEPLECHA, Z., 1970. Fireballs and the physical theory of meteors, *Bull. Astron. Inst. Czech.*, **21**, 271–296.

TABLE 1.—*Meteoroid With Initial Velocity $v_{\infty}=12$ km/s and Radius $R_{\infty}=100$ cm*

Velocity v (km/s)	Dynamical mass m_d (g)	Height H (km)	Epoch t (s)	Assumed heat-transfer coefficient Λ
5.000	6.0967×10^2	17.654	4.2592	0.00224
5.692	6.4917×10^2	17.999	4.1959	0.01734
6.446	7.8346×10^2	18.363	4.1370	0.03138
7.225	1.0994×10^3	18.750	4.0816	0.04458
7.980	1.7900×10^3	19.161	4.0286	0.05720
8.669	3.2799×10^3	19.601	3.9768	0.06952
9.268	6.4496×10^3	20.072	3.9253	0.08178
9.772	1.3035×10^4	20.570	3.8728	0.09426
10.191	2.6252×10^4	21.111	3.8184	0.10719
10.536	5.1745×10^4	21.706	3.7610	0.12082
10.822	9.9022×10^4	22.365	3.6994	0.13545
11.058	1.8352×10^5	23.104	3.6322	0.15140
11.255	3.2981×10^5	23.945	3.5576	0.16911
11.421	5.7708×10^5	24.920	3.4727	0.18922
11.561	9.8699×10^5	26.079	3.3737	0.21267
11.680	1.6587×10^6	27.506	3.2540	0.24100
11.780	2.7585×10^6	29.358	3.1011	0.27714
11.866	4.5839×10^6	31.994	2.8875	0.32754
11.939	7.7595×10^6	36.419	2.5258	0.41270
12.000	1.4661×10^7	73.536	0.0000	1.00000

TABLE 2.—*Meteoroid With Initial Velocity $v_{\infty}=12$ km/s and Radius $R_{\infty}=1000$ cm*

Velocity v (km/s)	Dynamical mass m_d (g)	Height H (km)	Epoch t (s)	Assumed heat-transfer coefficient Λ
5.000	4.3224×10^4	1.7160	5.2882	0.05170
6.281	8.8988×10^4	2.2542	5.2282	0.06718
7.454	2.4031×10^5	2.8161	5.1762	0.08050
8.408	7.1522×10^5	3.4026	5.1285	0.09263
9.145	2.0631×10^6	4.0220	5.0826	0.10425
9.708	5.4479×10^6	4.6686	5.0370	0.11574
10.144	1.3075×10^7	5.3541	4.9903	0.12742
10.487	2.8694×10^7	6.0834	4.9419	0.13949
10.762	5.8364×10^7	6.8585	4.8907	0.15215
10.987	1.1141×10^8	7.6891	4.8360	0.16561
11.174	2.0175×10^8	8.5869	4.7766	0.18011
11.330	3.4984×10^8	9.5653	4.7112	0.19596
11.463	5.8537×10^8	10.643	4.6380	0.21355
11.576	9.5153×10^8	11.699	4.5544	0.23343
11.674	1.5114×10^9	12.860	4.4564	0.25647
11.759	2.3604×10^9	14.281	4.3374	0.28406
11.832	3.6457×10^9	16.114	4.1851	0.31878
11.896	5.6144×10^9	18.698	3.9716	0.36624
11.952	8.7454×10^9	23.053	3.6087	0.44380
12.000	1.4661×10^{10}	73.532	0.0000	1.00000

TABLE 3.—*Meteoroid With Initial Velocity $v_{\infty}=30$ km/s and Radius $R_{\infty}=100$ cm*

Velocity v (km/s)	Dynamical mass m_d (g)	Height H (km)	Epoch t (s)	Assumed heat-transfer coefficient A
5.000	3.2649×10^{-5}	29.104	1.7436	0.01609
23.680	7.7116×10^{-1}	29.455	1.7215	0.02887
26.363	2.8707×10^1	29.826	1.7074	0.03705
27.493	2.2584×10^2	30.220	1.6934	0.04514
28.144	9.9065×10^2	30.641	1.6789	0.05352
28.571	3.1699×10^3	31.091	1.6637	0.06230
28.874	8.3382×10^3	31.576	1.6476	0.07159
29.101	1.9233×10^4	32.096	1.6303	0.08154
29.276	4.0281×10^4	32.646	1.6117	0.09226
29.416	7.8608×10^4	33.250	1.5914	0.10396
29.530	1.4512×10^5	33.919	1.5691	0.11683
29.623	2.5621×10^5	34.675	1.5442	0.13114
29.701	4.3758×10^5	35.540	1.5161	0.14733
29.766	7.2682×10^5	36.548	1.4837	0.16591
29.822	1.1836×10^6	37.757	1.4455	0.18784
29.870	1.9020×10^6	39.260	1.3988	0.21462
29.910	3.0356×10^6	41.235	1.3387	0.24899
29.945	4.8632×10^6	44.094	1.2542	0.29726
29.975	7.9709×10^6	49.320	1.1101	0.37931
30.000	1.4661×10^7	87.079	0.0000	1.00000

TABLE 4.—*Meteoroid With Initial Velocity $v_{\infty}=30$ km/s and Radius $R_{\infty}=1000$ cm*

Velocity v (km/s)	Dynamical mass m_d (g)	Height H (km)	Epoch t (s)	Assumed heat-transfer coefficient A
5.000	8.6440×10^{-4}	13.510	2.2721	0.01375
24.240	2.6803×10^3	13.855	2.2333	0.03189
26.458	6.9058×10^4	14.219	2.2193	0.03842
27.473	4.5678×10^5	14.605	2.2052	0.04498
28.083	1.7743×10^6	15.016	2.1907	0.05173
28.496	5.1904×10^6	15.455	2.1755	0.05881
28.799	1.2789×10^7	15.928	2.1593	0.06634
29.030	2.7879×10^7	16.438	2.1420	0.07438
29.211	5.5661×10^7	16.993	2.1234	0.08303
29.358	1.0420×10^8	17.600	2.1030	0.09246
29.479	1.8520×10^8	18.272	2.0807	0.10280
29.579	3.1676×10^8	19.024	2.0557	0.11433
29.664	5.2456×10^8	19.875	2.0276	0.12732
29.736	8.4820×10^8	20.838	1.9951	0.14225
29.798	1.3466×10^9	21.976	1.9568	0.15984
29.851	2.1108×10^9	23.377	1.9101	0.18126
29.897	3.2897×10^9	25.198	1.8499	0.20871
29.937	5.1470×10^9	27.790	1.7652	0.24718
29.971	8.2266×10^9	32.286	1.6207	0.31234
30.000	1.4661×10^{10}	87.077	0.0000	1.00000